

Influence of Cu Content on Microstructure and Corrosion Behavior of Flux-Cored Arc-Welded Metal with 10CrNi3MoV Steel

Jianglong Yi^{1,*}, Ben Niu¹, Rui Chen³, Yu Wang^{1,2}, Kai Wang^{2,**}, Yaoyong Yi¹

¹ Guangdong Provincial Key Laboratory of Advanced Welding Technology, Guangdong Welding Institute (China-Ukraine E. O. Paton Institute of Welding), Guangzhou, Guangdong, 510650, PR China

² Foshan University, Foshan, Guangdong, 528000, PR China

³ Hefei BOE Vision-electronic Technology Co.,Ltd, Hefei, Anhui, 230012, PR China

*E-mail: Yijl@gwi.gd.cn

**E-mail: hfutwk927@fosu.edu.cn

Received: 1 February 2019 / Accepted: 28 March 2019 / Published: 10 June 2019

This study aimed to investigate the effects of Cu addition on the properties of the 10CrNi3MoV steel weld metals prepared in the laboratory according to the flux-cored arc welding (FCAW) method. Specifically, the 10CrNi3MoV steel FCAW joints had been fabricated based on the as-prepared flux-cored wires after adding various Cu contents under the M21 mixed gas protection environment. Subsequently, the relationships of the micro-structural factors with the mechanical properties and corrosion behavior of the weld metal were examined through the metallographic, mechanical, EIS and SVET methods using the specimens cut transversely to the weld beads. Our research results had suggested that the addition of appropriate amount of Cu contributed to refining the grain size and improving the mechanical properties of the weld metals. Besides, it could also enhance the corrosion resistance of the FCAW welded metals, as verified through the conventional EIS and the localized microelectrodes (SVET) measurement.

Keywords: HSLA steel, Microstructure, Potentiodynamic polarization, Electrochemical impedance spectroscopy, Scanning vibrating electrode technique

1. INTRODUCTION

The 10CrNi3MoV high strength steel has been extensively applied in numerous industries, including pressure vessels, shipbuilding, offshore platforms, and marine structures, which can be ascribed to its superior physical properties, such as high yield strength, suitable toughness and excellent weldability [1,2,3]. The welding technologies including the keyhole deep penetration TIG and hybrid

laser/arc welding, have been advanced recently, which facilitates the production of various high strength steel weld structures and components [4,5]. However, the welded joints of those structures often used in seawater and related environments remain prone to corrosion, despite of the use of advanced weld processing techniques. Such phenomenon may be attributed to the following factors, (i) variation in composition, (ii) accumulation of residual stress, and (iii) modification in microstructure within the weld zone [6].

Notably, it is of vital significance for researchers to characterize, quantify, predict the corrosion behavior, and search for the potential way to prevent corrosion, since it is quite difficult and costly to repair the corroded parts of the high strength steel weld structures. Flux-cored arc welding (FCAW) is one of the most extensively applied welding techniques, particularly in the field of heavy plates welding, like shipyards and pressure vessels. A continuous tubular flux-cored wire will be fed to the molten pool during the FCAW process. Moreover, the composition of the welded metal can be easily altered through changing the alloy elements contained in the flux, thereby improving the corrosion resistance of the 10CrNi3MoV high strength steel welded metal [7].

So far, tremendous efforts have been made to investigate the welding process of 10CrNi3MoV the steel; however, those researchers and technicians mainly focus on the effects of various welding conditions on the mechanical and fatigue properties of the steel weld joints [3,8,9,10], while the electrochemical behaviors of 10CrNi3MoV steel, as well as the corresponding welds, have not been examined explicitly yet. For instance, Kai Wang et al. had reported the influence of the addition of different rare earth elements on the different mechanical and the electrochemical properties of the 10CrNi3MoV steel weld joints. Their research suggested that the appropriate addition of the REE to FCAW metals would enhance the mechanical properties and the corrosion resistance. The element Cu has been well recognized to boost the corrosion resistance. For instance, the addition of Cu into the ferritic, austenitic or duplex steels can positively affect the corrosion resistance in the sulfuric acid [11]. Nonetheless, the Cu addition amount must be under strict control based on the steel metallurgy principle, and excessive addition of Cu will negatively impact the physical properties of steel. Hence, this work aimed to examine the influence of Cu addition on the properties of the 10CrNi3MoV steel weld metals prepared through the FCAW process in the laboratory, especially for the correlation of Cu content with the corrosion behaviors. Our results would provide a probably efficient method for enhancing the corrosion resistance of the 10CrNi3MoV steel weld metals.

2. EXPERIMENT

Six different flux cored wires with the Cu content (200 μ m mesh, 99.9% purity) ranging from 0.0wt. % to 0.90wt. % (Table 1) had been fabricated using the XZ-YCX8 flux-cored wire production machine, among which, a cold-rolled strip was used as the sheath and a mixture powdered core, and the prepared flux-cored wire was 1.2 mm in diameter. The main composition of the slag forming materials was a rutile-fluorite alloying system, with the flux-cored filling ratio of 18%. Moreover, the 10CrNi3MoV high strength steel that was 300 mm \times 150 mm \times 15 mm in size had been utilized as the experimental base metal. The chemical composition and mechanical properties are listed in Table 2 and

Table 3, respectively. In addition, the welding machine (model: Taurus 421 forceArc DW, EWM company) had also been utilized to fabricate the welded joints. The welding parameters are displayed in Table 4.

Table 1. Main composition of the flux-cored wire with different Cu content (wt. %)

	Rutile	Fluorite	Ferrosilicon (75Si)	Ferromanganese (88Mn)	Nickel	Ferro- molybdenum	Copper	Atomized- Iron
Cu0	2.0	1.2	0.5	1.8	2.0	0.4	0.00	the rest
Cu1	2.0	1.2	0.5	1.8	2.0	0.4	0.15	the rest
Cu2	2.0	1.2	0.5	1.8	2.0	0.4	0.30	the rest
Cu3	2.0	1.2	0.5	1.8	2.0	0.4	0.45	the rest
Cu4	2.0	1.2	0.5	1.8	2.0	0.4	0.70	the rest
Cu5	2.0	1.2	0.5	1.8	2.0	0.4	0.90	the rest

Table 2. Chemical composition of the 10CrNi3MoV high strength steel

C	Si	Mn	Ni	Mo	Cr	V	P	S
0.11	0.31	0.39	2.72	0.23	1.05	0.88	0.010	0.005

Table 3. Mechanical properties of the 10CrNi3MoV high strength steel

Yield Strength/MPa	Tensile Strength/MPa	Elongation/%	A _k -20°C
590-745	670-850	≥16	≥80

Table 4. Parameters of Gas-shielding flux-cored wire welding

Protective gas	Gas flow rate (L/min)	Power Mode	Arc voltage V	Welding Current A	Welding speed mm/s	Heat input KJ/mm
M21(80% Ar + 20%CO ₂)	17~20	DCEP	23 ~ 24	230 ~240	5~6	0.94 ~1.03

within the range of 100 μm -140 μm using a video camera, the vibrating amplitude of the microelectrode was 30 μm , and the vibrating frequency was 80 Hz. Meanwhile, the scanning area on the working electrode surface was set as 5mm \times 5mm in the welded metals.

3. RESULTS AND DISCUSSION

3.1 Analysis of chemical composition

The chemical compositions of the series welded metals are displayed in Table 5. As could be observed, there were slight changes in the contents of Mn, Ni and Mo when different Cu contents were added. On the other hand, Cu addition would result in marked changes in the Si content.

Table 5. Chemical composition of the welded metals (wt. %)

Samples	C	Si	Mn	Mo	Ni	Al	Ti	Cu
Cu0	0.032	0.34	1.49	0.26	2.01	0.013	0.025	0.00
Cu1	0.034	0.32	1.43	0.22	2.04	0.011	0.030	0.11
Cu2	0.029	0.29	1.56	0.24	2.00	0.0098	0.024	0.28
Cu3	0.036	0.34	1.49	0.21	2.02	0.012	0.029	0.50
Cu4	0.033	0.49	1.53	0.25	2.00	0.020	0.034	0.72
Cu5	0.037	0.48	1.47	0.20	2.03	0.020	0.045	0.89

3.2 Microstructures of the welded metals

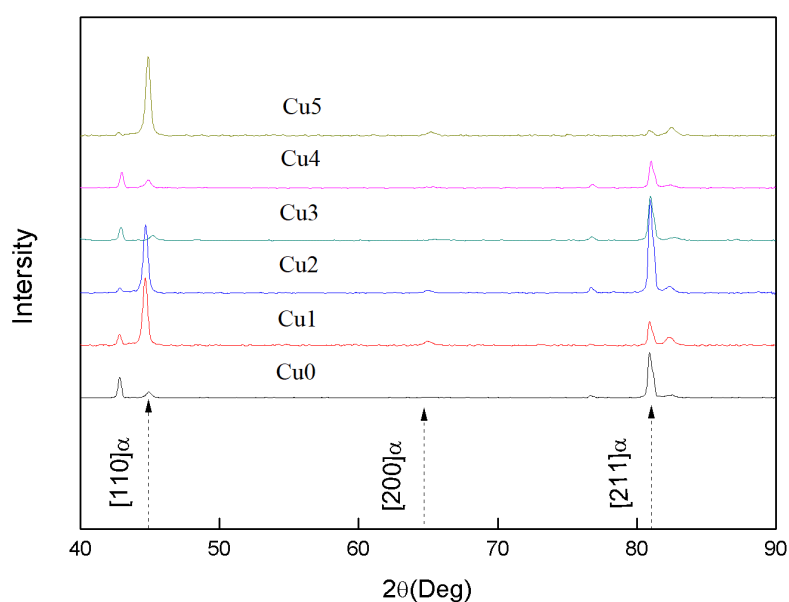


Figure 2. X-ray diffraction patterns of the six welded metals with different Cu contents

The results of X-ray diffraction for each sample are shown in Fig.2. As could be observed, those welded metals were mainly composed of the α -Fe phase, and no new phase was formed with the increasing Cu content.

The metallographic structures of the welded metals under different Cu addition amounts are presented in Fig.3. Obviously, all welded metals had a major structure of pro-eutectoid ferrite and bainite, which was not similar to that depicted in our previous research [12] where no bainite was formed with REE addition.

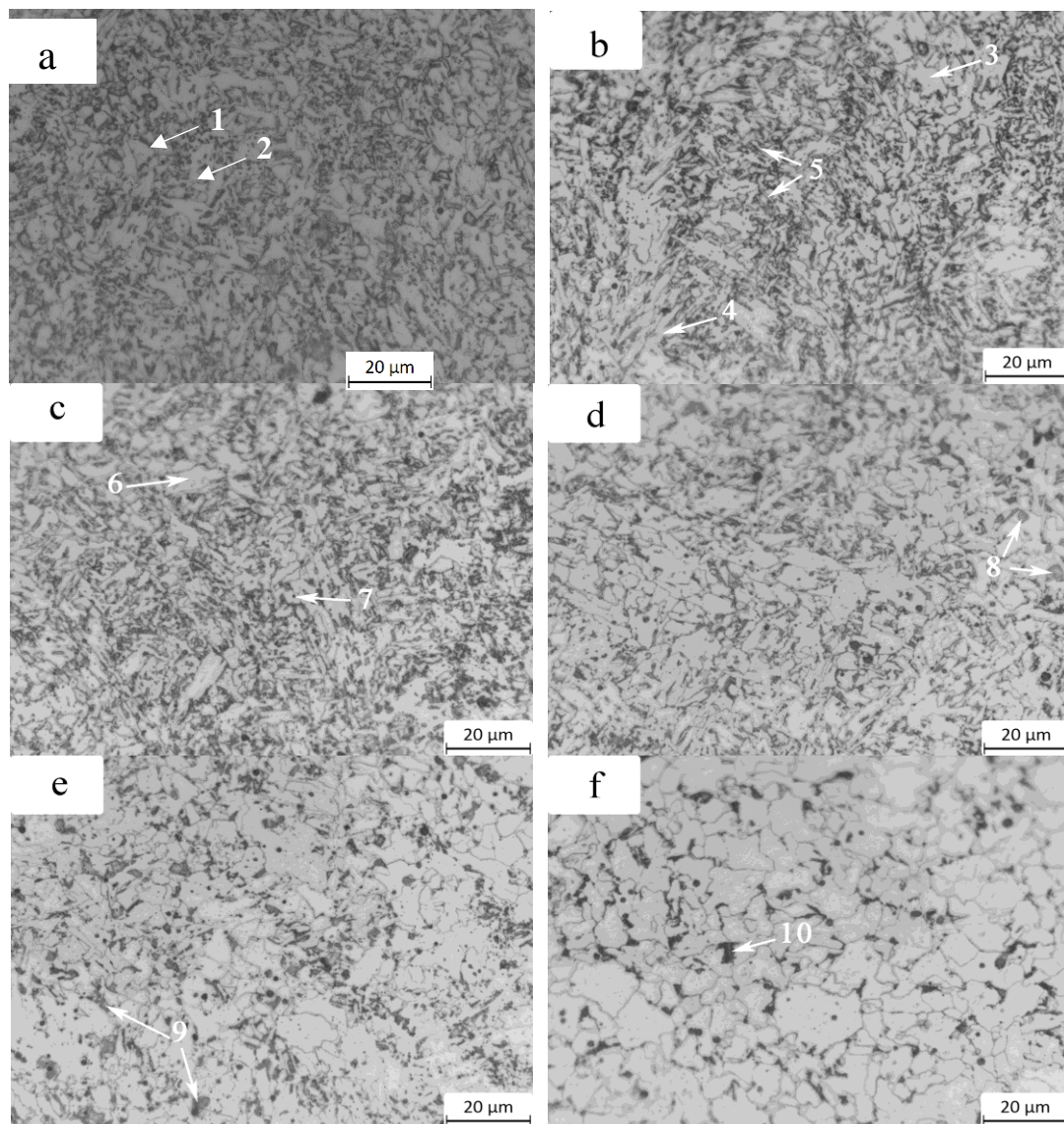


Figure 3. Metallographic structures of the six welded metals with different Cu contents: (a) Cu0 (b) Cu1,0.11wt. % (c) Cu2, 0.28wt. % (d) Cu3, 0.5wt. % (e) Cu4, 0.72wt. % (f) Cu5, 0.89wt. %

Typically, the microstructure of the welded metal had consisted of the coarse block pro-eutectoid ferrite (PF, 1) and granular bainite (GB, 2) [Fig.3(a)] in the absence of Cu, among which, the lighter blocks represented the aggregates of ferrite grains, and some darker granular bainite was distributed

inside the ferrite. Meanwhile, the grain morphology and size in Cu0 samples were not uniform. Typically, the metallographic structure of the welded metals would change obviously with the increase in Cu content. For the welded metal Cu1 with 0.11% Cu content, the microstructure was composed of block PF (3), lath ferrites (LF, 4), acicular ferrites (AF, 5) and bainite. For the welded metal Cu2 with 0.28% Cu content, the LF structure was reduced, and the microstructure mainly consisted of plenty of AF and bainite, with less block PF (6) and GB (7). Additionally, a structure of the more refined grains could be obtained, as displayed in Fig.3(b) and Fig.3(c). Specifically, AF growth and the grain refinement effect could be attributed to the addition of Cu based on two aspects. On the one hand, as one of the austenite stabilization elements, Cu could slow down the steel transformation from austenite to ferrite and pearlite [13,14]; on the other hand, Cu addition could delay the recrystallisation and grain growth during the cooling process [15]. Moreover, the total amount of grain boundaries would sharply increase with the formation of AF and the refined grain size, which could enhance the resistance to dislocation motion and plastic deformation, finally leading to the enhanced strength and resistance to crack growth [16,17,18].

Cu precipitates could be observed in the welded metals when the Cu content had reached 0.5wt. %, as marked in Fig.3 d, e, f (8, 9, 10); besides, the amount of gray aggregates and total grain size would elevate with the increasing Cu content. In addition, grain morphology and size became non uniform and coarse when the Cu content had approached 0.89wt. %. Cu had limited solubility in iron; therefore, the Cu precipitates would be accumulated in the grain boundary when the Cu content had exceeded 0.5wt. %, which would render the distorted crystal lattice surrounding the Cu aggregates and the increased inner micro-stresses [19]. In the meantime, the Cu precipitates might reduce the mechanical and electrochemical properties of the welded metals.

3.3 The mechanical properties of the welded metals

The mechanical properties of the FCAW welded metals performed at room temperature are exhibited in Fig.4. It could be noted from Fig.4a that, the values of tensile strength (R_m) and yield strength (R_e) had increased after Cu addition. In addition, it could be clearly seen that, when the Cu content had increased from 0 to 0.28wt. %, both the yield strength and tensile strength would remarkably increase. Specifically, the tensile strength could reach the maximum value of 727MPa at the Cu content of 0.5wt. % in the welded metal. However, the value of tensile strength began to decrease at the Cu content of >0.72wt. %, but it was still higher than that of the copper-free FCAW welded metal. Such variation trend was similar to that of the yield strength test results, which had displayed a peak value of 657MPa at the Cu content of 0.28wt. %. As could be observed from the microhardness results in Fig 4b, the microhardness of the six welded metals varied from 232 to 256 HV0.3, which had slightly fluctuated at the Cu content of ≤ 0.5 wt. %. However, the value of microhardness would suddenly decrease when the Cu content had reached 0.7wt. %.

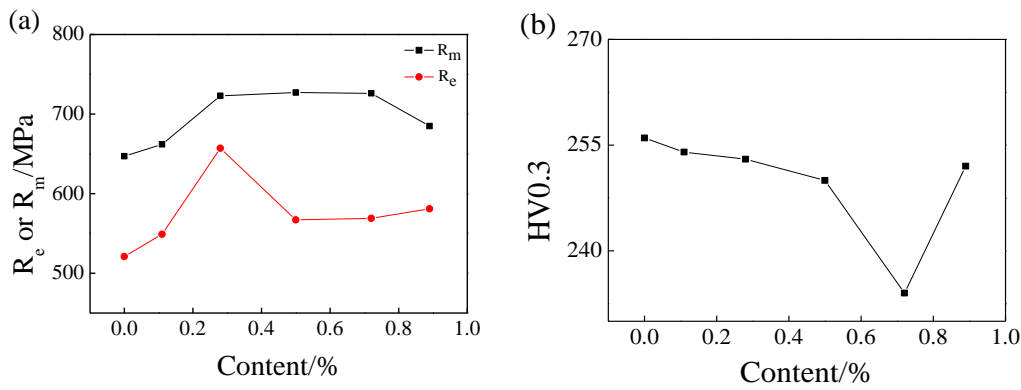


Figure 4. Effect of Cu addition on the (a) yield strength (Re) and tensile strength (Rm), as well as the (b) microhardness

10CrNi3MoV is the well-known high strength steel, which is frequently utilized to build constructional structures. Therefore, the welded metal of this steel should necessarily have a low yield ratio (which represents a ratio of yield strength to tensile strength) as well as a low temperature toughness. Fig.5 depicts the variation trends of the yield ratio and the Charpy impact energy at -40 °C. At the Cu content of 0.5wt. % to 0.7wt. % in the weld deposits, Cu addition would result in an acceptably low yield ratio. Nevertheless, Cu addition would exert negative effect on the Charpy impact energy, and the copper-free welded metal would have the highest impact energy (40J, tested at -40°C).

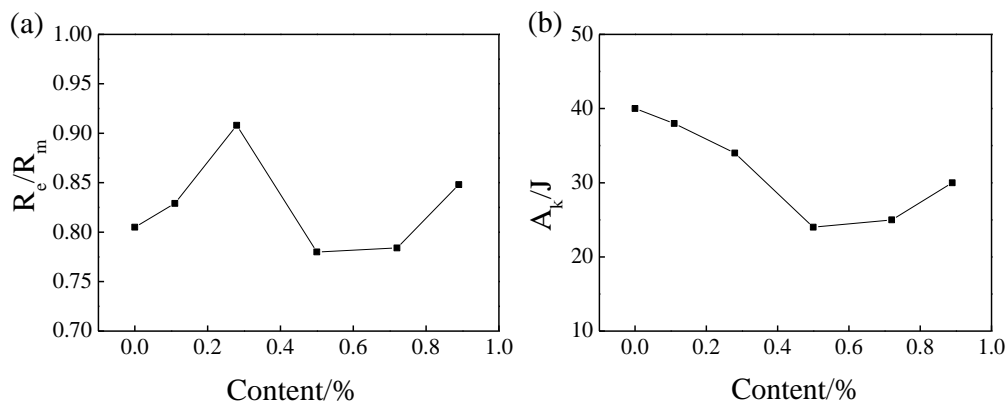


Figure 5. Effect of Cu addition on the(a) yield ratio and the (b) Charpy impact energy at -40 °C

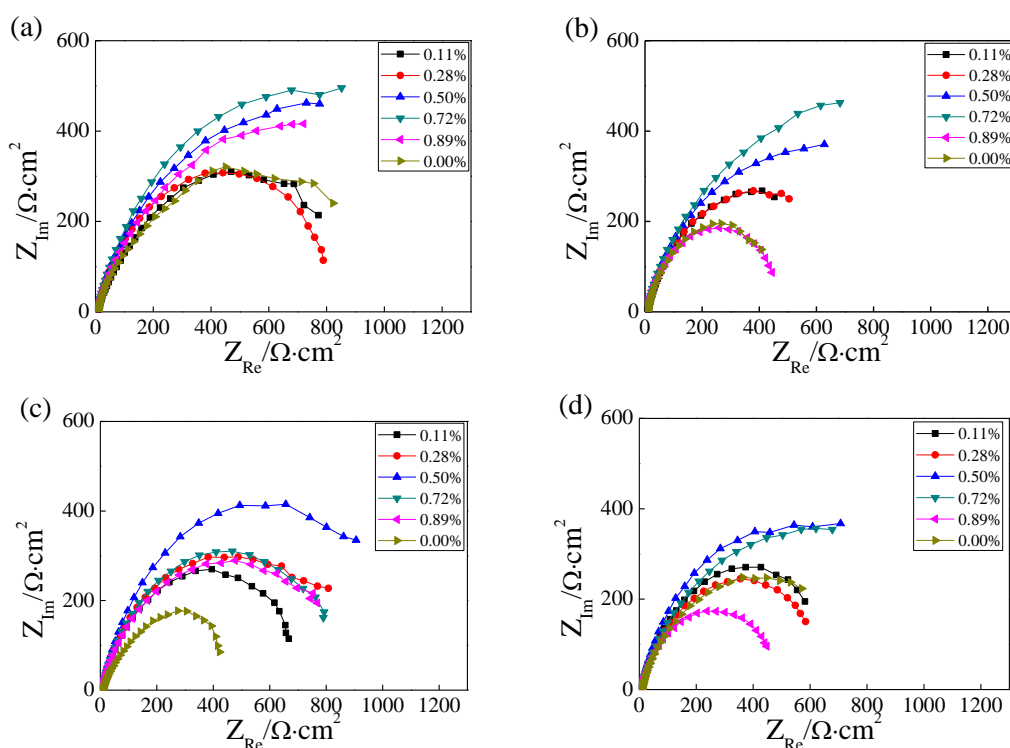
Based on the above mechanical properties of the six FCAW welded metals, Cu content of 0.5wt. % would lead to more effective strengthening effect, and such increase in strength might be attributed to the solid solution strengthening as well as the grain refinement under Cu addition, as observed in other studies [20,21]. For the ferrite steel, the strengthening mechanisms had been identified as the solid-solution strengthening and grain-refinement strengthening, as indicated by Eq.(1) [22,23].

$$\begin{aligned} \Delta\sigma_y &= \Delta\sigma_0 + \Delta\sigma_{SS} + \Delta\sigma_{GB} & (1) \\ &= 53.9 + (32.34[Mn] + 83.1[Si] + 360.36[C] + 354.2[N] + 33[Ni] + 40[Cu]) \\ &\quad + 17.402d^{-1/2} \end{aligned}$$

where $\Delta\sigma_y$ was the yield strength, $\Delta\sigma_0$ was the strength of the pure iron, $\Delta\sigma_{SS}$ and $\Delta\sigma_{GB}$ represented the contributions of solid-solution strengthening and grain-boundary strengthening, respectively, while d stood for the average diameter of the ferrite grain [24]. As could be observed from Fig.3, a more refined structure of the FCAW welded metal could be obtained when the Cu content was appropriately increased. The reason why Cu addition at ≤ 0.28 wt. % would sharply increase the yield strength could be easily figured out from the above microstructure and mechanical analyses. Moreover, the grain size and microstructure would obviously change at the Cu content of >0.5 wt. %, while the yield strength would decrease.

3.4 Electrochemical properties of the welded metals

Fig.6 has presented the Nyquist plots regarding the experimental impedance spectra obtained with different welded metals exposed to 3.5 wt.% NaCl at different immersion time periods. Specifically, the Nyquist plots of all the welded metals had exhibited a complete capacitive reactance, which was indicative of the presence of the time-constant electrode processes; for example, $R_s(R_{ct}Q_{dl})$, where R_s was the solution resistance, while R_{ct} and Q_{dl} represented the charge-transfer resistance and double layer capacitance, respectively. In addition, the single capacitive semi-circle also indicated that the corrosion process was mainly controlled by the charge transfer [25]. On the other hand, the real part diameter of the semicircle in the Nyquist plots had represented the anti-dissolution properties. Fig. 6 suggested that the corrosion resistance of the welded metals was increased with the increase in Cu addition. All the semi-circle diameters in the Nyquist plots had gradually decreased with the increase in immersion time, except for the welded metal with 0.89wt. % Cu content, whose EIS spectral shape showed noticeable fluctuant change.



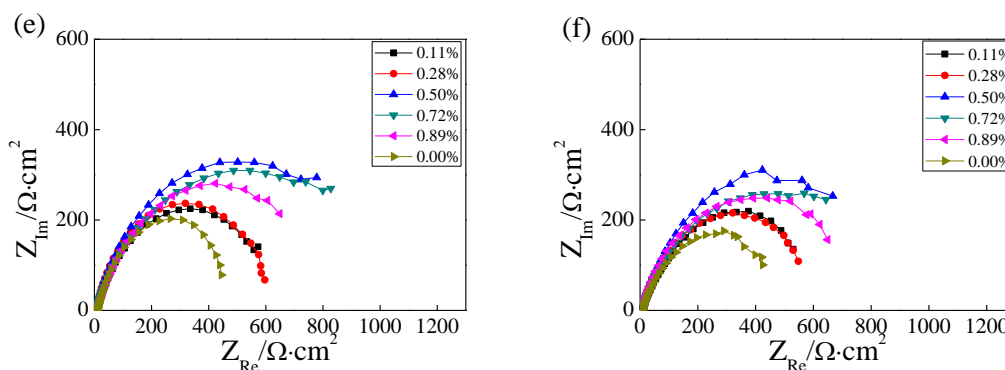


Figure 6. Nyquist plots of the six welded metals with different Cu contents after different immersion times in 3.5% NaCl. (a) 24h (b) 48h (c) 72h (d) 144h (e) 240h (f) 336h.

For the copper-free welded metal, the capacitive response was effectively independent of the immersion time. Besides, when the FCAW welded metal with 0.72wt. % Cu content was immersed in the aqueous 3.5% NaCl solution from 24 h to 48 h, the Nyquist had exhibited the largest semicircle diameter. As the immersion time extended from 72 h to 336 h, the welded metal with 0.5wt. % Cu addition had presented the largest capacitive arc, which indicated that the protective film formed on this weld deposits had become more stable than others with the extension of time. Taken together, the above EIS test results had demonstrated that Cu addition would boost the corrosion resistance of the FCAW welded metals.

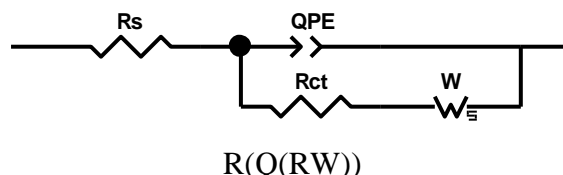


Figure 7. Equivalent circuit used to model the experimental EIS data.

The equivalent circuit $R(Q(RW))$ shown in Fig.7 was used to simulate the welded metal corrosion in the NaCl solution. R_s representing the solution resistance, R_{ct} is the charge-transfer resistance, Warburg impedance (W) is considered to the diffusion resistance. The fitting results are listed in Tab.6, and the respective errors are below 1%. The Cu4 sample with 0.72wt. % Cu content has the highest R_{ct} value at the beginning of the corrosion test. As the immersion time extended to 240 h, the welded metal with 0.50wt. % Cu content (Cu3 sample) change to has the highest R_{ct} value.

Table 6. Impedance parameters for the EIS-tested welded metals.

Time	Samples	R_s ($\Omega \cdot \text{cm}^2$)	CPE ($S \cdot \text{sec}^n$)	Freq Power (n)	R_{ct} ($\Omega \cdot \text{cm}^2$)	Warburg ($S \cdot \text{sec}^5$)	Chi-squared
24h	Cu0	7.157	0.0008922	0.7603	842.2	0.00712	0.01361
	Cu1	7.613	0.001221	0.7349	915.7	0.04637	0.01156
	Cu2	7.936	0.0007561	0.8096	829.2	8.634E9	0.004786
	Cu3	7.945	0.0008615	0.8089	941.8	0.003899	0.009117

	Cu4	7.948	0.0006402	0.8225	1165	0.003593	0.01553
	Cu5	7.63	0.00142	0.7791	851.6	0.003629	0.01285
48h	Cu0	6.915	0.0006029	0.8267	622.6	4.783E10	0.005883
	Cu1	7.918	0.001545	0.7486	647.8	3.015E6	0.002986
	Cu2	7.799	0.00243	0.7691	514	1.456E8	0.005223
	Cu3	7.491	0.0009101	0.7955	865.1	0.01096	0.008086
	Cu4	8.521	0.002107	0.7167	862.5	6.794E16	0.006244
	Cu5	7.614	0.001002	0.774	788.3	0.007968	0.01443
72h	Cu0	6.972	0.001078	0.7908	764.8	0.02138	0.002796
	Cu1	7.485	0.001261	0.7944	720.4	0.2079	0.004091
	Cu2	7.72	0.001287	0.8078	780.3	0.01526	0.003169
	Cu3	7.554	0.00125	0.8186	1079	0.07361	0.007185
	Cu4	7.524	0.002428	0.7007	501.8	1.294E10	0.00557
	Cu5	7.598	0.0008287	0.8074	828.3	0.0272	0.01028
144h	Cu0	6.494	0.003273	0.7166	517.5	6.047E5	0.003379
	Cu1	7.569	0.003032	0.7013	675.6	2.802E11	0.005241
	Cu2	7.478	0.002211	0.7758	597	0.2075	0.00726
	Cu3	7.311	0.002989	0.7545	884.7	7.364E7	0.007053
	Cu4	7.502	0.002212	0.7691	627.9	0.01598	0.008528
	Cu5	8.236	0.001614	0.7884	650.6	0.03067	0.01345
240h	Cu0	7.248	0.005112	0.7554	648.6	0.07945	0.007087
	Cu1	7.219	0.00407	0.775	761.1	3.783E6	0.004794
	Cu2	6.972	0.002806	0.7849	652.3	0.09834	0.007319
	Cu3	7.027	0.003183	0.8013	935.5	0.02105	0.005716
	Cu4	7.541	0.003532	0.7835	765.3	0.01318	0.017077
	Cu5	6.738	0.003209	0.7702	503.2	1.697	0.001621
336h	Cu0	8.189	0.005759	0.7693	740.9	0.08017	0.006975
	Cu1	7.549	0.003798	0.7999	802	0.01187	0.0034.7
	Cu2	7.947	0.004727	0.7845	733.9	0.1225	0.005216
	Cu3	7.005	0.004561	0.788	504	0.1516	0.002912
	Cu4	7.301	0.003391	0.808	802.4	0.006669	0.0036
	Cu5	7.593	0.00286	0.8036	495.5	3.433E7	0.007466

Potentiodynamic polarization measurements had also been performed in the 3.5% NaCl solution at room temperature under different immersion times. The typical anodic and cathodic polarization curves, as well as the polarization parameters are illustrated in Fig.8 and Table 7, respectively. As displayed in Fig.8, the presence of Cu would affect both the cathodic and anodic tafel lines, which also indicated that both the anodic and cathodic processes would be controlled by the charge-transfer processes, and such findings were consistent with those from previous Nyquist analysis. Fig. 8a revealed that, the potentiodynamic polarization curve had shifted to the more negative direction with the increase in Cu content after being immersed in NaCl solution for 24 h. As the immersion time extended, all the corrosion potentials had shown the more negative values, which might be resulted from the formation of the oxide layer that could provide the barrier to the oxygen reduction reaction [26]. Fig.8a has also compared the polarization curves among various welded metals. As could be observed, the current density would no longer increase with the potential during anodic polarization when the Cu addition

amount had reached 0.89wt. %; instead, it maintained at a relatively stable value, indicating that the passive film could only be formed at this Cu addition content.

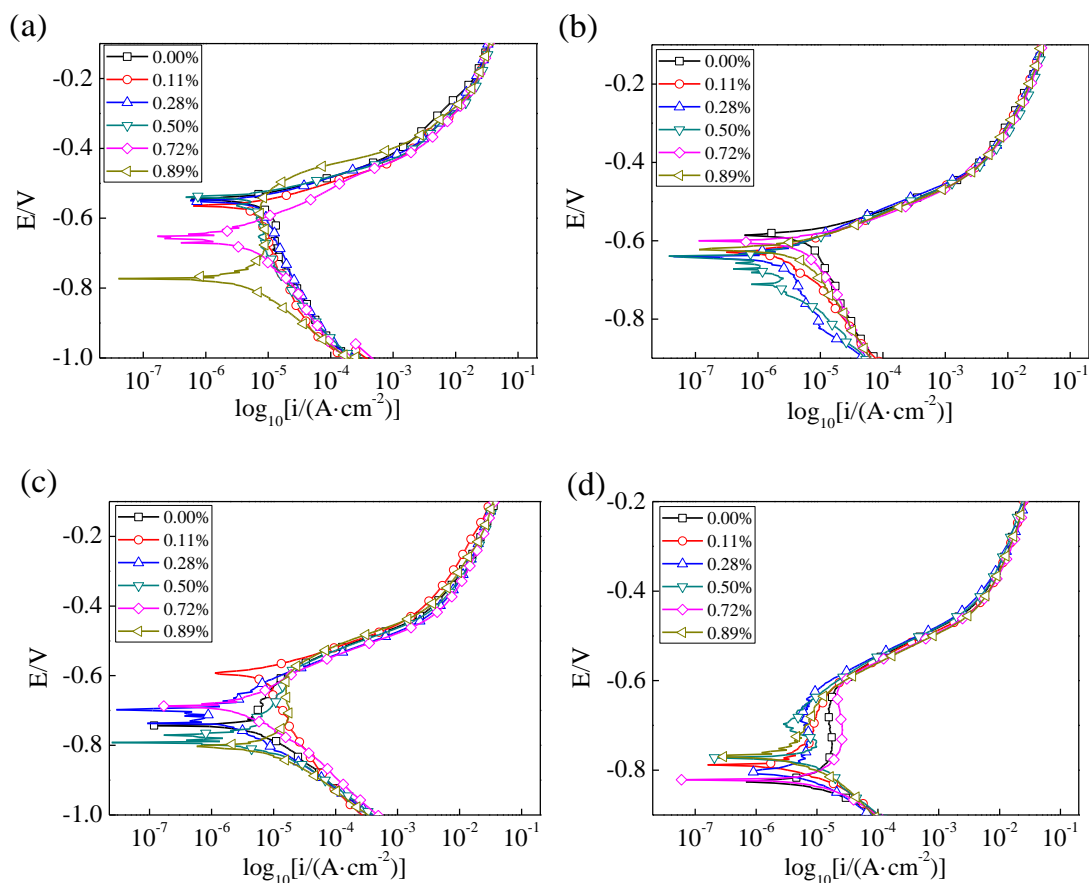


Figure 8. Potentiodynamic polarization curves of the six welded metals under different Cu contents after being immersed for different times in 3.5% NaCl. (a) 24h (b) 72h (c) 144h (d) 240h

In Table 7, the E_{corr} was the corrosion potentials, which represented the corrosive susceptibility, while the I_{corr} represented the corrosion current densities, which served as a key factor to the corrosion-dissolution rate of a material. Apparently, the corrosion current densities were more intense for the copper-free welded metal under different immersion times compared with the Cu-added specimens, suggesting that Cu addition could reduce the I_{corr} value and enhance the corrosion resistance of the FCAW welded metals in 3.5 wt. % NaCl solution. After 24 h of immersion, the test specimen with 0.5 mt% Cu content had the lowest E_{corr} and I_{corr} values, which had the strongest corrosion reduction effects.

Table 7. Potentiodynamic polarization parameters of different welded metals

Immersion time (h)	Samples	Cu Content(%)	E_{corr} mV _{SCE}	I_{corr} μ Acm ⁻²
24h	Cu0	0.00	-0.546	13.4
	Cu1	0.11	-0.565	10.5
	Cu2	0.28	-0.548	8.37

	Cu3	0.50	-0.540	8.14
	Cu4	0.72	-0.651	1.03
	Cu5	0.89	-0.773	2.20
72h	Cu0	0.00	-0.586	9.08
	Cu1	0.11	-0.629	3.13
	Cu2	0.28	-0.641	2.01
	Cu3	0.50	-0.641	0.628
	Cu4	0.72	-0.602	1.48
	Cu5	0.89	-0.622	2.99
144h	Cu0	0.00	-0.743	14.1
	Cu1	0.11	-0.591	8.96
	Cu2	0.28	-0.697	0.0312
	Cu3	0.50	-0.775	0.0652
	Cu4	0.72	-0.687	2.97
	Cu5	0.89	-0.802	22.9
240h	Cu0	0.00	-0.822	19.4
	Cu1	0.11	-0.789	11.2
	Cu2	0.28	-0.797	6.60
	Cu3	0.50	-0.731	0.241
	Cu4	0.72	-0.82	2.03
	Cu5	0.89	-0.766	6.66

3.5 SVET characterization

Fig. 9 shows the SVET maps for measuring the welded metals, which can test the local corrosion potential under the specimen surface. The 3D maps had clearly shown that, the copper-free welded metal had the higher susceptibility to corrosion in the NaCl solution. Besides, the current density had displayed the obvious trend of first decrease and then increase as the Cu content had increased. As shown in Fig. 8 (c), the minimum average value of current density for the welded metal (approximately $19 \mu\text{A}/\text{cm}^2$) with 0.28wt. % Cu content had exhibited the best corrosion performance. When the Cu content had increased from 0.5wt. % to 0.89wt. %, the maximum current density had sharply increased, which would no longer change with the increase in Cu addition and maintain at an average value of about $54 \mu\text{A}/\text{cm}^2$, indicating that the addition of excessive Cu might not improve the corrosion resistance of the welded metals.

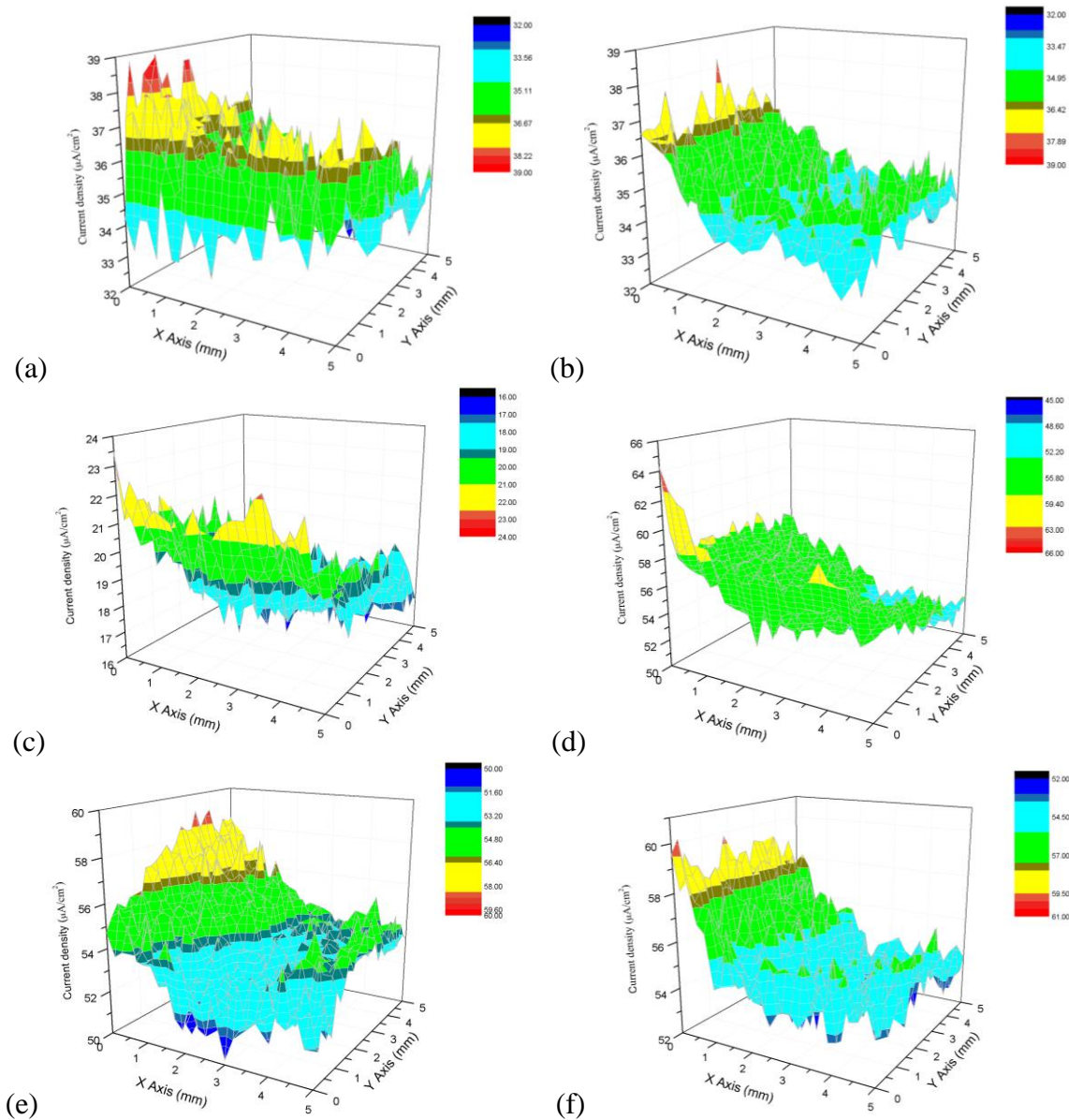


Figure 9. SVET maps of different welded metals after 12 h of immersion in the 3.5 wt. % NaCl solution: (a) Cu0 (b) Cu1, 0.11wt. % (c) Cu2, 0.28wt. % (d) Cu3, 0.5wt. % (e) Cu4, 0.72wt. % (f) Cu5, 0.89wt. %

It could be seen from Fig.9 (a) to (d) that, the distribution of corrosion currents became more uniform as the Cu content had increased from 0wt. % to 0.5wt. %, which was consistent with the microstructure results. Moreover, the welded metal with 0.5wt. % Cu addition had exhibited the higher maximum corrosion current value, but it had the best homogeneous distribution of corrosion current density, which suggested that a uniform oxide had been formed on the welded metal surface. Typically, the increased corrosion current density might contribute to the formation of a large amount of acicular ferrites. Besides, the acicular ferrite morphology was associated with less exposure area to the corrosive medium, which might thereby affect the reduction reaction in NaCl solution [26, 27].

4. CONCLUSIONS

The effects of Cu addition on the microstructure and corrosion behaviors of the FCAW metal with 10CrNi3MoV steel have been investigated through the scanning vibrating electrode technique (SVET) as well as other conventional measurement techniques, and the following conclusions can be summarized:

(1) The six different welded metals possess similar major microstructures of the pro-eutectoid ferrite and bainite. Besides, the increase in Cu addition from 0wt. % to 0.5wt. % can refine the grain size and promote the growth of acicular ferrites. Cu precipitates can be observed in the welded metals when the Cu content has reached 0.5wt. %; in addition, the grain morphology and size have become non-uniform and coarse when the Cu content is further increased to 0.89wt. %.

(2) Results of mechanical analysis reveal that Cu addition at the level of ≤ 0.28 wt. % can sharply enhance the yield strength, which will be decreased at the Cu addition of > 0.5 wt. %. Nevertheless, Cu addition will negatively affect the microhardness and the Charpy impact energy.

(3) According to EIS results, the appropriate Cu addition amount can improve the corrosion resistance of the FCAW welded metals, which is achieved through increasing the semi-circle diameter in Nyquist plot; thus, the corrosion potentials (E_{corr}) will be shifted to the more negative values and the corrosion current densities will be lowered (I_{corr}). After 24 h of immersion, the test specimens with 0.5 wt% Cu addition has the lowest E_{corr} and I_{corr} values, which has displayed the greatest corrosion reduction effect.

(4) Results of local electrochemical SVET test indicate that, the distribution of corrosion currents becomes more uniform when the Cu content has increased from 0wt. % to 0.5 wt. %. Specifically, the welded metal with 0.28 wt. % Cu addition has the lowest maximum corrosion current density ($23\mu\text{A}/\text{cm}^2$); meanwhile, the test specimen with 0.5 wt. % Cu content has the most homogeneous distribution of corrosion current density.

(5) It can be discovered that Cu should be added within a content rang of 0.3wt. %-0.45wt. %, so as to achieve sufficient effect and obtain the optimal microstructure, mechanical and corrosion properties for the 10CrNi3MoV steel welded metal.

ACKNOWLEDGEMENTS

This work was supported by GDAS' Project of Science and Technology Development (2017GDASCX-0113, 2016GDASPT-0205), the technical project of Guangzhou (201704030112, 201604046026, 201508030024), and the technical project of Guangdong (2017A070701026, 2014B070705007).

References

1. A.Akyel, M.H.Kolstein, F.S.K.Bijlaard, *Journal of Constructional Steel Research*, 139 (2017) 374.
2. W. Song, X. S. Liu, F. Berto, S.M.J. Razavi, *Materials*, 661 (2018) 1.
3. X.Z. Chen, Y.M. Huang, Y. C. Lei, *Journal of Alloys and Compounds*, 631 (2015) 225.
4. S.W. Cui, Y.H. Shi, K. Sun, S.Y. Gu, *Materials Science and Engineering: A*, 709 (2018) 214.
5. M. Mazar Atabaki, N. Yazdian, R. Kovacevic, *Advances in Manufacturing*, 6 (2018) 176.
6. G. Pimenta and T. A. Jarman, "The corrosion of metal joints, chapter 3-35, corrosion and degradation of engineering materials," in Shreir's Handbook of Corrosion, 3rd edition (2010) 2447.
7. D. Katherasan, J. V. Elias, P. Sathiya, A. N. Haq, *Journal of Intelligent Manufacturing*, 25 (2014)

- 67.
8. K. Peng, C. L. Yang, C. L. Fan, S. B. Lin, *The International Journal of Advanced Manufacturing Technology*, 96 (2018) 677.
 9. K. Peng, C. L. Yang, C. L. Fan, S. B. Lin, *Journal of Materials Processing Technology*, 251 (2018) 225.
 10. K. Peng, C. L. Yang, S. B. Lin, C. L. Fan, Y. Q. Han, M. P. Wu, *The International Journal of Advanced Manufacturing Technology*, 93 (2017) 967.
 11. X. Y. San, B. Zhang, B. Wu, X. X. Wei, E. E. Oguzie, X. L. Ma, *Corrosion Science*, 130 (2018) 143.
 12. K. Wang, Q. Lu, Y. Yi, J. Yi, B. Niu, Z. Jiang, J. Ma, *International Journal of Corrosion*, (2018) 1.
 13. C. Hsu, K. Lin, *Materials science and engineering A*, 528 (2011) 5706.
 14. D. Isheim, S. Vaynman, M. Fine, D. Seidman, *Scripta Materialia*, 59 (2008) 1235.
 15. S. Wang, Q. Wang, H. Wang, F. Liu, et al, *Materials science and engineering A*, 743 (2019) 197.
 16. C. Zhang, X. Song, P. Lu, X. Hu, *Materials and Design*, 36 (2012) 233.
 17. B. Basu, R. Raman, *Welding Journal*, 81 (2002) 239s.
 18. G. Spanos, R. W. Fonda, R. A. Vandermeer, et al. *Metallurgical and Materials Transaction A*, 26A (1995) 3277.
 19. I. Altpeter, G. Dobmann, K. Kakerbau, M. Schick, et al, *Nuclear Engineering and Design*, 206 (2001) 337.
 20. B. Mishra, K. Kumbhar, K. S. Kumar, K. S. Prasad, M. Srinivas, *Materials Science & Engineering A*, 651 (2016) 177.
 21. S. Wang, Q. Wang, H. L. Wang, F. P. Liu, W. J. Yao, F. Jiang, J. Sun, F. Y. Wang, *Materials Science & Engineering A*, 743 (2019) 197.
 22. H. W. Yen, P. Y. Chen, C. Y. Huang, J. R. Yang, *Acta Mater*, 59 (2011) 6264.
 23. F. B. Pickering, *Physical Metallurgy and the Design of Steels*, Applied Science Publishing Ltd., London, 1978, p. 63.
 24. Y. Q. Wang, X. M. Zhang, Z. He, G. Q. Zu, G. F. Jia, J. Y. Duan, R. D. K. Misrac, *Materials Science & Engineering A*, 703 (2017) 340.
 25. H. Nady, M. M. El-Rabiei, M. Samy, *Egyptian Journal of Petroleum*, 26 (2017) 79.
 26. K. M. Deen, R. Ahmad, I. H. Khan, Z. Farahat, *Materials and Design*, 31 (2010) 3051.
 27. S. P. Kumaresh Babu, S. Natarajan, *Materials and Design*, 29 (2008) 1036.